Experimental investigation of condensation heat transfer in small arrays of PCM-filled spheres

M. M. WEISLOGEL and J. N. CHUNG

Department of Mechanical and Materials Engineering, Washington State University, Pullman,
WA 99164-2920, U.S.A.

Abstract—Experimental investigations on the condensation heat and mass transfer between flowing steam and a small regularly packed bed of encapsulated spheres filled with PCM (phase-change material) are performed. The objectives of the research are to obtain transient transport characteristics of the dual-latent heat thermal storage system during the charging process. A special device is used to instrument the inside of the sphere. This device retards the sinking of the unmelted solid PCM toward the bottom of the spherical shell, thus reducing the strong dependence of the heat flux on tangential angle location. Instantaneous heat transfer rates are obtained for spheres of three different sizes (with single sphere and small packed bed arrangements). Tests performed to note Reynolds number and Stefan number dependencies of the two phase transfer and energy storage are also carried out. The device worked well, particularly for the larger spheres (6.35 and 7.62 cm diameter), which allowed the normalized thermal energy stored to be correlated by a single dimensionless time scale for all of the tests performed.

1. INTRODUCTION

ENERGY management systems are being used by industrial commercial establishments and military operations to reduce their overall energy consumption. Quite often many different sources and demands for energy exist and the total energy usage of the system can be reduced by the utilization of the waste heat from one or more processes as an energy source for others. Since the availability and the demand for the thermal energy may not coincide time-wise, the flexibility of the energy utilization system can be greatly increased by the development of an efficient method for storing thermal energy to insure the continuity of the thermal process.

Thermal energy storage can also be used to reduce the mass of the heat rejection system. Waste heat generated during high-power sprint mode operation is absorbed by the thermal storage unit and then later dissipated over a much longer non-operation period.

There are many methods available for the storage of thermal energy. Among them, the packed bed deserves some attention due to its large interfacial transport areas during processing. For example, in a space-based thermal system, a thermal storage unit with high-energy storage density over a narrow temperature range is highly desirable. Under such requirements, a packed bed of spheres filled with a phase-change material (PCM) coupled with a phase-change liquid (preferably metal) working fluid is thought to be a best qualified candidate. This paper documents the results of an experimental project which is aimed at understanding the basic heat and mass transfer mechanisms in a dual-latent heat packed bed thermal storage system.

In the literature, a considerable amount of work is concerned with the heat and mass transfer in packed beds used as chemical reactors. Those reports mainly focus on the steady operation of the process. Here we restrict our review to only the packed beds in thermal storage systems. Most of the investigations have been analytical and numerical. The majority of the work has focused on the one-dimensional, time-dependent, separated two-medium model first developed by Schumann [1] for fairly simple initial and boundary conditions. Schumann's model predicts the mean solid and fluid temperatures as a function of the axial location and time. Schumann's model was extended and modified by many researchers to include variations in inlet conditions, two-dimensional effects, and wall effects [2–7]. On the experimental investigations, a series of experiments was performed by Peavy and Dressler [8] who considered transpiration heat transfer of water in a sand column. Jones and Hill [9] investigated the transport of heat in a pebble-bed using air as the working fluid. Similar experiments were performed by Beasely and Clark [10].

So far we have reviewed only the transport in packed beds with no phase-change in either the working fluid or the bed materials. Next we examine the previous work on packed beds of PCM with single-phase working fluid. Yimer *et al.* [11] and Kordahi *et al.* [12] have performed numerical simulations of the melting process inside an encapsulating material. Torab and Beasely [13] employed a finite-difference method to study the dynamic response of a packed bed with PCM. On the experimental side, the work by Pal [14] provides a good data set for a cylindrical bed packed with PCM-filled spheres undergoing charging and cooling processes for step inlet con-

NOMENCLATURE

Material and thermophysical properties

c_p specific heat [J kg^{-1} $^\circ$C^{-1}]
h_{fg} latent heat of vaporization [J kg^{-1}]
h_{sf} latent heat of fusion [J kg^{-1}]
k thermal conductivity [W m^{-1} $^\circ$C^{-1}]
m mass [kg]
α thermal diffusivity, $k/\rho c_p$ [m^2 s^{-1}]
β thermal expansion coefficient [$^\circ$C^{-1}]
v kinematic viscosity [m^2 s^{-1}]
ρ mass density [kg m^{-3}].

Important quantities and dimensions

D diameter [m]
E energy [J]
E' average energy required per degree
         increase in temperature [J $^\circ$C^{-1}]
g acceleration due to gravity, 9.812 m s^{-2}
h heat transfer coefficient [W m^{-2} $^\circ$C^{-1}]
$\dot{m}''$ mass flux [kg m^{-2} s^{-1}]
q instantaneous energy transferred [W]
R sphere radius [m]
t time [s]
T temperature [$^\circ$C]
X thickness of encapsulating shell [m]
δ thickness of the condensate film
ε voidage, or porosity.

Calculated quantities

$\bar{c}_p$ specific heat corrected for change in
         phase
E^* normalized energy, E/E_{scale}
         [dimensionless]
q'' average heat flux
t^* normalized time, t/t_{scale} [dimensionless]

ΔT $T_f - T_i$
ΔT_1 $T_f - T_m$
ΔT_s $T_m - T_s$
θ center temperature convergence
         criterion, $(T_c - T_i)/(T_f - T_i)$.

Subscripts

ave   average value
c   center of sphere
conv   convection
eff   effective value
exp   experimental value
f   final, energy storage process complete
film   condensate film
i   initial, energy storage begins
l   liquid
m   melt, quantity evaluated at melt
         temperature
pcm   property or dimension of PCM
s   solid
shell   encapsulating shell property
sph   sphere
theo   theoretical value
tot   total for system.

Equations and dimensionless groups

Bi_{eff} Biot number based on sphere radius,
         hR/k_{eff}
Fo Fourier number, $\alpha t/R^2$, or $(k/R)t/(\rho c_p R)$
Ja Jakob number, $c_p \Delta T/h_{fg}$
Re_D Reynolds number, $2VR/v$, or $2\dot{m}''R/\mu$
Ste Stefan number, $\rho_l c_p \Delta T_1/\rho_s h_{fg}$.

ditions (temperature and mass flux) with air as the working fluid. Graves [15] attempted an experimental investigation, yet was frustrated by leaking PCM packings and, hence, an unknown working fluid. Limited reports were found concerning the heat and mass transfer of condensing working fluid in a packed bed or tube bundles. Thomas [16] experimentally examined the transport mechanisms in a packed bed of solid spheres. The direct-contact condensation rate of upward flowing vapor on downward flowing liquid films that coat the packing surfaces was measured. Based on the experimental data, useful correlations were also provided. Instead of packed beds, extensive and valuable contributions were made toward the enhancement of condensation on the tube bundles by Marto and his co-workers. Marto [17] summarized the results.

Although with its many potential benefits, the packed bed of PCM with condensing working fluid (dual-latent system) has not been treated in the litera-

ture. Only recently has a finite-difference numerical model been used to study the fluid flow and heat and mass transfer in a dual-latent packed bed system [18]. A parametric study was performed in ref. [18] because of a lack of information on the heat transfer coefficient between the condensing fluid and the bed of encapsulated spheres with melting inside. It is the intent of the current paper to provide that heat transfer information through careful experimentation.

The following is a list of the specific results obtained in this research work.

(1) The instantaneous heat transfer rates between the condensing fluid and the PCM inside the sphere.
(2) The effects of the size of the encapsulated sphere on the heat and mass transfer rates.
(3) Scaling relationships indicating physical dependencies on system dimensions and thermophysical properties.

Only charging processes were investigated.
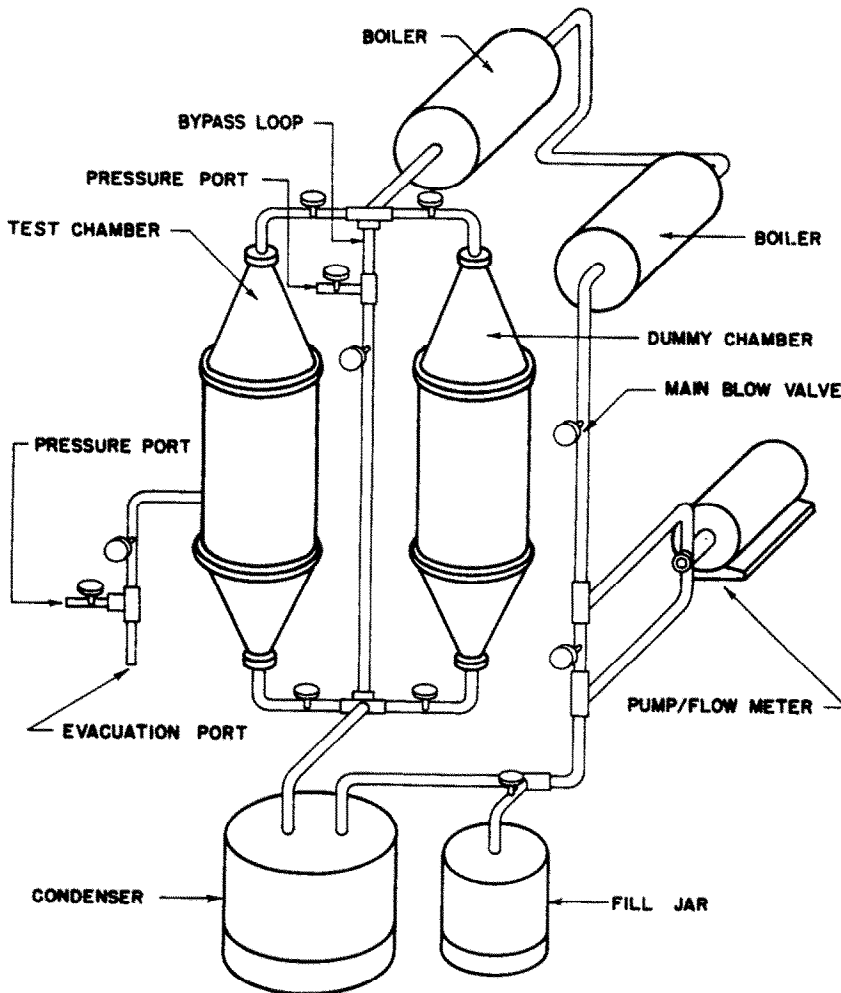
FIG. 1. Schematic of experimental apparatus.

2. EXPERIMENTAL APPARATUS

The main objective of the apparatus was that it be able to produce a clean, non-condensible gas-free environment which could, as rapidly as possible, provide a steady *ambience* for an isolated PCM-filled sphere, or array of spheres, in terms of pressure, temperature, and velocity (or mass flow rate), so that the energy transfer characteristics of the process could be observed.

2.1. *Components of the experimental system*

A general schematic of the experimental apparatus employed in this study is provided as Fig. 1. The primary thermal loop, capable of both opened and closed cycle operation, consists of a metering flow pump (by which the flow rate of vapor was determined), two boilers in series, a dummy chamber to establish the working fluid condition, a test chamber to house the spheres under study, and a simple coil-type condenser.

Chambers and sphere holders. The aluminum cham-

bers were identical in geometry except for a few access ports on one. O-Ring seals allowed for moderately high vacuum conditions. Both chambers were leak tested to less than 100 μm Hg. A more detailed schematic of this part of the cycle is provided as Fig. 2 with dimensions given in centimeters. Wire screens in the entrance cones of each chamber acted to shed to the perimeter of the main chamber bodies any condensate which might have otherwise come in contact with the spheres or ambient temperature and pressure probes.

As pictured in the figure, aluminum sphere holders were designed and fabricated which could be inserted into the test chamber. Each of these holders was intended to support the single sphere and multiple sphere arrangements and was sized accordingly. The spheres of the arrayed tests were supported on the sides by the aluminum insert and on the bottom by steel rods which were isolated thermally by wrapping them in 3 mm tygon tubing. The chambers and sphere holders were made of 3 and 1.5 mm thick sheet, respec-
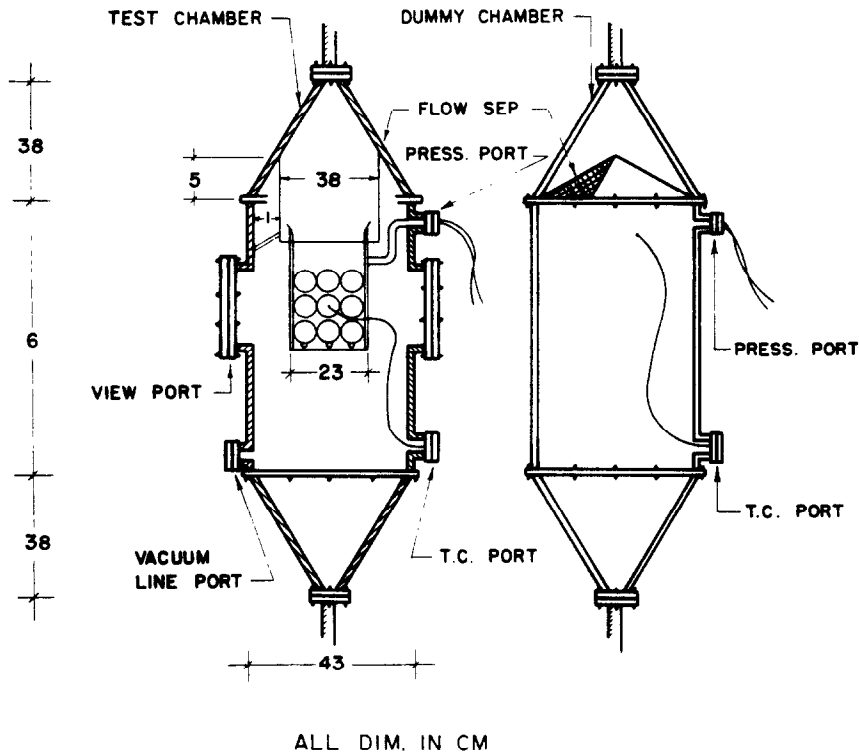
FIG. 2. Schematic of chamber detail with dimensions given in centimeters (note: a $3 \times 3 \times 3$ array of 7.62 cm diameter spheres is shown in the figure).

tively. Both chambers were insulated with thermal blankets to minimize wall condensation and heat loss to the surroundings.

2.2. *Measurements and calibration*

Transient and steady pressures were measured using pressure transducers, tested for linearity and re-calibrated with a mercury manometer to improve on the accuracy determined by the manufacturer.

Type-T 36 gauge thermocouple wire was used for the majority of the temperature measurements, except for in the cases of the heat flux transducer calibration experiments where 0.0762 mm diameter wire was used for improved time response.

The PCM-encapsulating spherical shells consisted each of 304 stainless steel. The PCM selected for this series of tests was a paraffin, P-116. The relevant thermophysical properties for each material are listed in Table 1, along with the important system dimensions. Properties of the wax determined specifically for this experiment are also provided in the table, namely the thermal expansion coefficient (β) and the kinematic viscosity (v) of the material, the latter is presented graphically as a function of temperature in Fig. 3.

The spherical shells themselves varied in thickness depending on the diameter of the particular sphere. These thicknesses were 0.51, 0.61, and 1.02 mm for

the 5.08 cm (2 in.), 6.35 cm (2.5 in.), and 7.62 cm (3 in.) diameter spheres, respectively. Each sphere was fitted with a thread to mate with 3 mm long 304 stainless steel machined screws which provided for time efficient sealing of the spheres and for material continuity.

The non-instrumented spheres were injected with liquid PCM at about 120°C until the fluid brimmed the sphere. The stainless steel screws, wrapped with teflon tape, were then inserted into nylon washers and tightened down into the fittings of each sphere. The warm nylon washer when squeezed between the screw head and the sphere provided a leak proof seal. Since the spheres were completely filled with liquid PCM, a relatively high vacuum (at least 100 μm Hg—the apparent vapor pressure of P-116) was drawn upon solidification of the wax. If the seal was not perfect, air would be sucked into the shell which would then result in a pressurized sphere during the next melt cycle. Random spheres were thus leak tested in hot oil and observed for escaping air. No leakage was noticed for oil bath temperatures 50°C beyond the liquid fill temperature. Spheres weighed before and after particular experiments showed no PCM loss which has been a problem in past studies, particularly by Graves [15], and much less so by Pal [14].

The instrumented spheres were treated similarly as

Table 1. Thermophysical properties for SS and P-116 (PCM), and other relevant system constants and dimensions (mass of machined stainless steel screws, 4.7 g)

Material and/or phase	ρ (kg m^{-3})	c_p (J kg^{-1} °C^{-1})	k (W m^{-1} °C^{-1})	ν ($\times 10^7$ m^2 s^{-1})	β ($\times 10^4$ °C^{-1})	h_{fg}[b] (kJ kg^{-1})
304SS	7900	477	14.9	—	—	—
PCM$_l$ (at T_m)	786	2270	0.15	—	[a]	210
PCM$_l$ (78°C)	729	—	0.15	4.83	9.843	210
PCM$_s$ (at T_m)	817	2890	0.22	—	—	210
Steam liquid (103°C)	957	4220	0.681	—	—	2252
Steam vapor (103°C)	0.635	—	—	—	—	2252

Sphere diameter (cm)	Shell thickness (± 0.05 mm)	Mass SS shell (± 2 g)	Mass PCM (± 2 g)	Void fraction[c] ε_{sph}	Inlet area (m^2)
5.08	0.51	39	43	0.146	0.0232
6.35	0.61	89	90	0.129	0.0363
7.62	1.02	132	162	0.140	0.0523

[a] β determined experimentally as function of temperature.
[b] h_{sf} implied where necessary.
[c] Averaged value over at least four spheres.

the non-instrumented spheres only a special screw was fabricated so as to permit the temperature at the center of the sphere to be measured. A schematic of this arrangement is included as Fig. 4. Holes drilled in the stainless steel screws at 90 deg allowed for the fine thermocouple wire to pass through and into the center of the sphere. The lead wire of the thermocouple was sandwiched between two nylon washers which, when squeezed, provided the necessary seal. Hollow ceramic dowels glued to the screw tips guided the thermocouples directly to the center of the spheres where they remained for the duration of each test regardless of the churning effects of the melting process. Feathered nylon bushings were fitted to the tips of the dowels for added grip with the PCM solid. The bushing would delay the sinking of the unmelted solid mass to the bottom of the shell such that the heat flux would remain relatively uniform over the sphere surface. Sealing against leakage for these spheres was more difficult than for the non-instrumented spheres, yet eventually a 'perfect' seal could be achieved for each sphere.

A number of heat flow sensors (Microfoils, heat flux transducers (HFT)) were purchased from the RdF

FIG. 3. P-116 kinematic viscosity dependence on temperature.

Corporation for the purpose of monitoring the energy transferred to the spheres during the experiments. The dimensions of each transducer were 6.35 mm by 17.78 mm, the area of the actual heat flow measurement being roughly 6.35 mm by 6.35 mm.

The material used as the substrate in which the thermopiles were imbedded was Kapton, with a thermal conductivity of 0.118 W m^{-1} °C^{-1}. Since the thermal impedances of the heat flux transducer substrate and the combination of the sphere wall and the PCM differed greatly (304 SS ; k = 14.9 W m^{-1} °C^{-1}), separate calibration experiments needed to be conducted in order to determine a multiplication constant for the linear output of the gauge. Each sensor was received with individual specifications concerning μvolt output per heat input, response time, dimensions, and dependence on temperature data, the latter which was fit by a fifth-order polynomial and incorporated into the data acquisition system.

Two means of calibrating the transducers were used in conjunction. The first employed a comparison between the heat flow sensor and a thermocouple pair measurement technique for a thick stainless steel plate exposed to a condensing steam jet.

In these tests, an intrinsic thermocouple pair (0.0762 mm diameter), one on either side of the 6.35 mm stainless steel plate, was attached next to a heat flux transducer. A steam jet was then directed at the plate and the output of the transducer and thermocouples were recorded in time. The output temperature values of the thermocouple pair were then fed into a numerical routine which employed a Crank–Nicolson scheme to solve inversely for the instantaneous heat flux. These values were then compared to the output of the HFT and a multiplication factor (MF) was calculated based on the integrated heat flux values (or energy transferred). Typical plots of these experiments are provided as Figs. 5 and 6, the latter presenting the results of the former multiplied by an
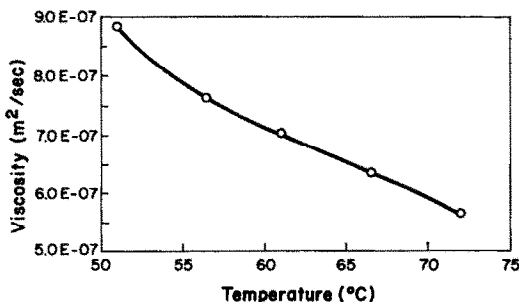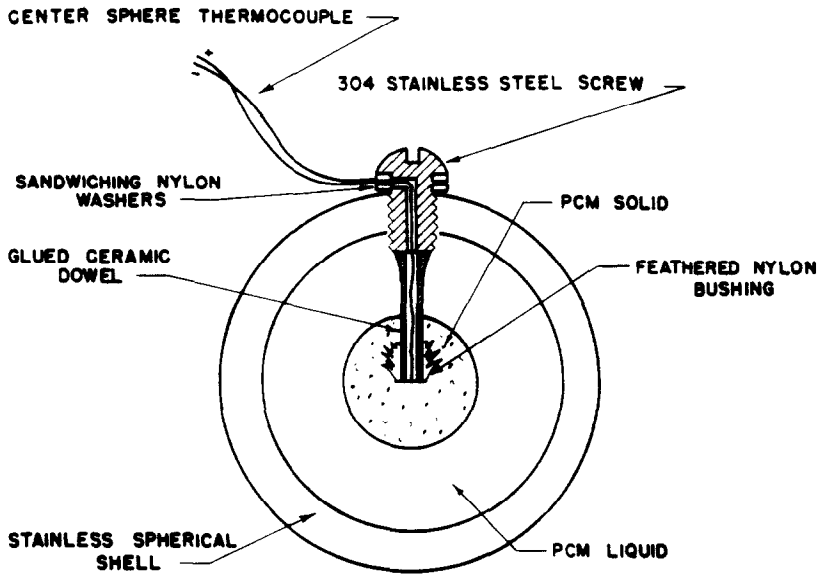
FIG. 4. Sketch of center temperature measurement technique (note : shell thickness greatly exaggerated).
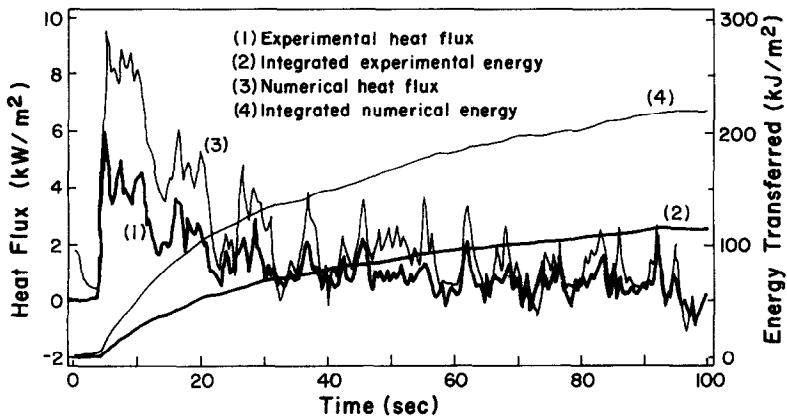
FIG. 5. Calibration plots for heat flux transducer output and thermocouple isolated pair (for data taken at 0.5 s intervals and multiplication factor of 1.0).
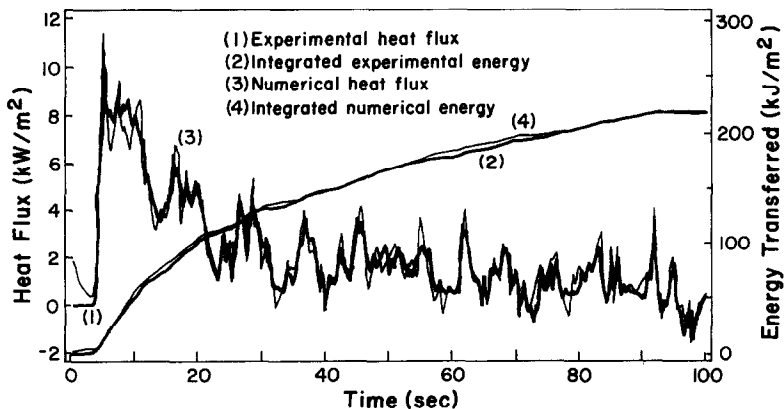
FIG. 6. Calibration plots for heat flux transducer output and thermocouple isolated pair (for data taken at 0.5 s intervals and multiplication factor of 1.916).

experimentally determined constant—in this case, $MF = 1.916$. The software used for this calibration procedure was verified to produce extremely accurate results when compared to analytical solutions, for the most part deviating less than 1% with oscillations less than 0.07%. One can note from these plots that the heat flow sensor's output was very sensitive to the irregular heat flux inputs of the condensation heat transfer process.

Since the heat transferred into the PCM was also a function of the wall thickness and a slight function of the heat transfer rate,† the MF arrived at through these means needed to be validated.

A parallel means to converge more precisely to the correct multiplication factor for a given experiment was to ratio the summed heat fluxes over time, generated by the heat flux transducer, to the analytically determined total energy considering the thermodynamic initial and end states. The dowels used to measure the center temperatures acted to even out the heat flux in the tangential gradient. Under normal gravity conditions, the PCM solid would settle to the bottom of the sphere where it would create a nonuniformity by increasing the heat flux over the lower portion of the sphere via direct contact between the hot shell wall and PCM solid. The center temperature probe with feathered nylon bushing prevented this from occurring by maintaining the solid at the center of the sphere during most of the energy-storing period of the PCM. This phenomenon was verified by visualizing the melting process through a transparent glass sphere. Gravitational effects were therefore limited to natural convection in the liquid PCM. This smoothing out of the heat flux over the sphere enabled single heat flux transducer measurements to be far more representative of the average heat flux to the sphere in time. Though the heat flux still varied over the surface of a given sphere, an estimation of the overall heat flux history of the sphere could be traced-out by multiplying the experimental energy transferred by the ratio of the total possible thermodynamic energy storable to the total experimental energy stored, given an initial and final state—both in temperature and phase, or

$$MF \int_{t_i}^{t_f} q_{exp}\, dt = E_{theo}$$

where q_{exp} is known experimentally as a function of time and E_{theo} is the theoretical energy stored by the sphere. Figure 7 displays this technique for heat flux measurements made at four significantly different tangential angle locations on a 7.62 cm diameter sphere immersed in a constant temperature water bath. It can

be observed from the figure that a 'bowing' of the energy storage history is prevalent about some likely straight line, roughly the curve traced out by line 3. Since it was speculated that the energy storage rate of the sphere would have a large linear region [19], this particular tangential angle of approximately 120 deg from the top of the sphere was selected for all of the tests. Because this angle could not be meticulously maintained the multiplication factor varied slightly from case to case. One will note these values range in the vicinity of those found experimentally by the previous method, namely 2.0. Thus, multiplication factors used in this study were determined using this technique and are listed with each plot of results where relevant.

3. PROCEDURES AND RESULTS

3.1. Preparatory procedure

The steps to ready the system for the actual data taking were straightforward, consisting primarily of system evacuation and subsequent flush/filling with degassed water to aid in removing non-condensible gases.

While the fluid was circulating through the bypass loop, the preheater and boiler were turned on until saturated steam at slightly above atmospheric conditions was generated. This also helped guarantee a minimum of noncondensibles in the fluid transport lines of the thermal loop. The valve to the bypass loop was then closed and the inlet valve to the dummy chamber was opened. The chamber was allowed time to pressurize until it too reached slightly elevated atmospheric saturation conditions. The exit valve of the dummy chamber was then opened which enabled the fluid to circulate again.

While steady conditions were being reached in the dummy chamber, evacuation continued on the test chamber. The evacuated test chamber pressure was typically around 380 μm Hg.

3.2. Inlet conditions technique

Once the circulating fluid reached and maintained steady conditions in the dummy chamber loop, a 'burst' method was used to transfer these conditions to the test chamber. This method involved closing the exit valve to the dummy chamber once it had reached the steady flow condition. Steam pressure in the dummy chamber was allowed to build to a prescribed value whereupon the inlet valve to the test chamber was opened. At this time, not only did the test chamber receive vapor generated by the boilers, but also the excess vapor stored in the previously pressurized dummy chamber. The dummy chamber entrance valve was closed at another predetermined pressure, while the exit valve of the test chamber remained closed so that build-up to the steady conditions could proceed. Once this condition was reached the test chamber exit valve was opened and the flow was established, now in the test chamber loop. The inlet trans-

---

† The heat flux transducer's thermal capacitance adds a complication when the device is used for transient measurements. Numerous experiments have shown a slight, and hence negligible, influence due to the transients of the sensors themselves.
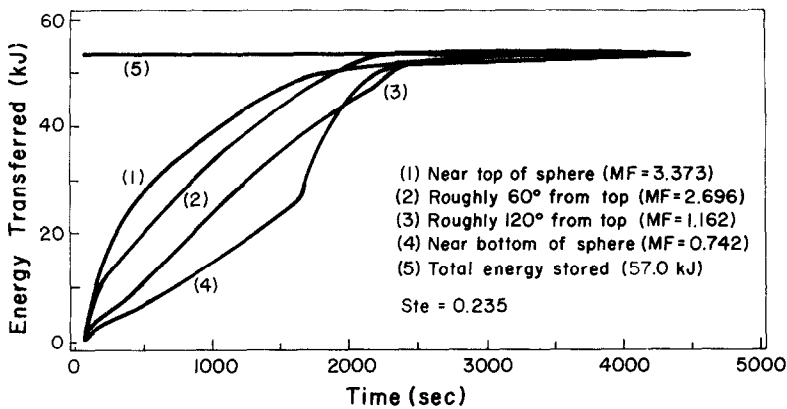
FIG. 7. Tangential angle dependence of heat transfer for a 7.62 cm diameter sphere immersed in a constant temperature bath.

port line from the boiler to the test chamber was preheated by a heating tape to a temperature slightly higher than the steady flow condition temperature. This process had a negligible effect on increasing the temperature of the test chamber before the test and helped guarantee that a minimum of condensate would enter the chamber. Data sampling began normally 30 s before the inlet to the test chamber was opened. The heat flux measurements, relevant temperatures, and pressures were sampled every second for as long as necessary. Evacuation of the test chamber was terminated less than 5 s before the inlet valve to the test chamber was opened.

The burst technique was used in each of the dual latent experiments performed in this study, except for a few of the higher flow rate tests where the sink potential of the test chamber became less significant.

Slightly distinct changes in the instantaneous heat flux for particular runs were noticed at the point where the exit valve of the test chamber was opened allowing the flow to circulate. This was because of the increased convection which was quantified by the integrated heat flux data.

3.3. Experiments

The first series of experiments involved a certain sphere (or sphere configuration), instrumented with a heat flux transducer, a sphere surface thermocouple, and a center sphere thermocouple, which was filled with solid PCM and placed in the test chamber. Opening the inlet valve to this chamber began the energy transfer process between the condensing steam and the melting PCM.

In order to develop a better understanding of the effects of neighboring spheres in a packed bed experiencing dual latent heat transfer, a comparison approach was intended. This approach entailed gathering data for single isolated spheres of varying diameters and comparing it to the data for the same spheres in an array of identical spheres of the same diameters, holding the inlet conditions constant. Supplementary tests on a small packed bed were also performed to

monitor the axial dependence of the energy storage process. The tests involved cubic sphere stackings of $3 \times 3 \times 3$ (three axial layers) and $3 \times 3 \times 6$ (six axial layers), where two or three spheres were instrumented with HFTs at varying axial positions.

A final series of immersion tests were performed by simply 'dipping' an instrumented sphere into a water bath at various temperatures and recording the transient flux and temperature data. These tests were undertaken to document the effect of a varying Stefan number ($\rho_l c_p \Delta T_l / \rho_s h_{sf}$) on the exchange process. Stefan numbers of 0.560, 0.283, and 0.103 were achieved for these experiments.

3.4. Data and integrated flux results

Dual latent heat transfer tests. Typical data resulting from a selected dual latent energy exchange test in the chambers are presented graphically in Figs. 8 and 9. Figure 8 displays the raw heat flux and significant temperature data while Fig. 9 plots the integrated heat flux over time for the center sphere of a $3 \times 3 \times 3$ array of 7.62 cm (3 in.) diameter spheres. The data presented here well represents, with regard to general trends, those obtained for all cases. It will be seen later that the bulk of the experimental results could be more concisely and simply presented.

Analysis of Fig. 8 reveals a relatively steady heat transfer process with a curious center temperature profile in time. This temperature increased quite rapidly in all tests at a certain time late in the experiment when the suspension of the PCM solid could no longer be maintained. Though repeatable, this phenomena was undesirable, but was seen not to affect the heat flux histories significantly since the mass of the dropping PCM solid was small. The 5.08 cm (2 in.) spheres tested were most affected as was the sphere used for the immersion tests which required suspension times of up to 2.5 h. Figure 9 reveals the energy storage history of the process as being relatively steady.

These behaviors were characteristic of each exper-
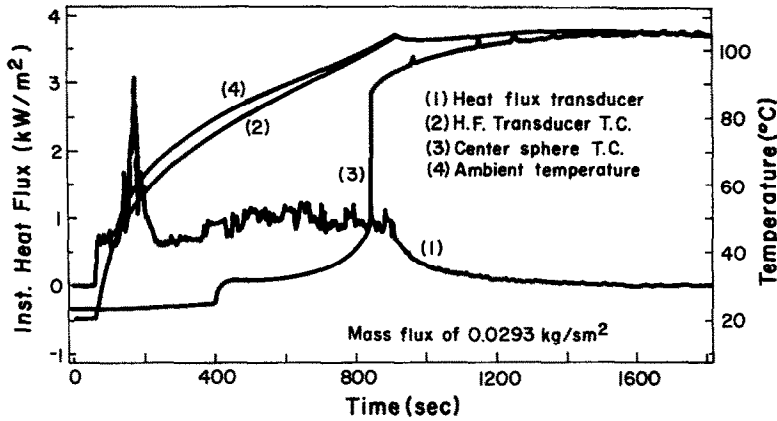
FIG. 8. Plots of temperature and heat flux data with time for 7.62 cm diameter arrayed sphere (data taken at 1 s intervals).
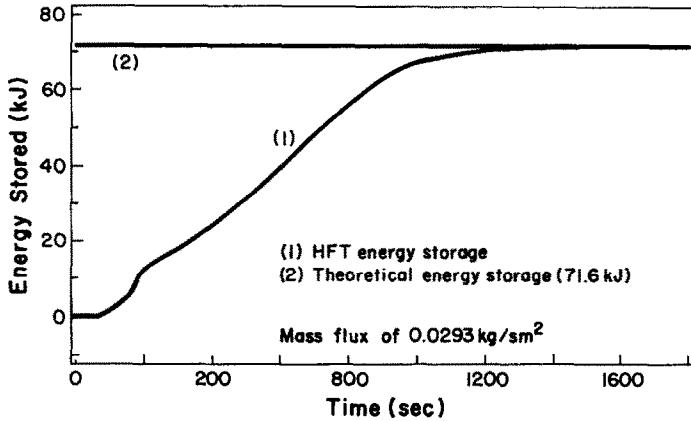
FIG. 9. Plots of experimentally integrated energy for 7.62 cm diameter arrayed sphere (data taken at 1 s intervals).
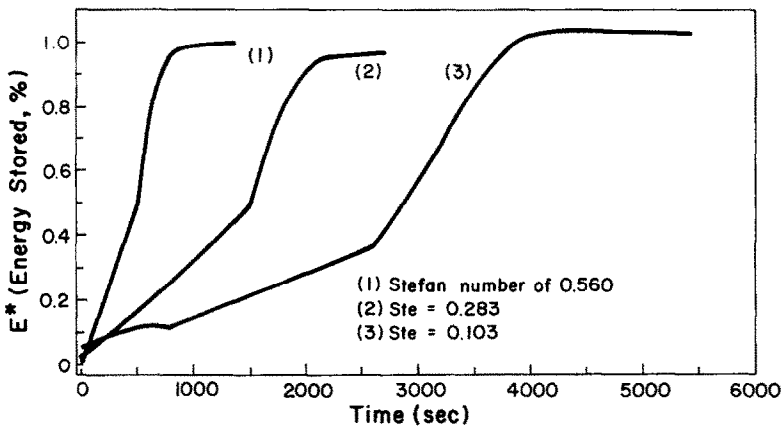
FIG. 10. Plots of normalized energy vs time for immersed sphere tests (for 7.62 cm diameter spheres).

iment which could easily be repeated and shown to reproduce practically identical results.

Immersion tests. The immersion tests to note Stefan number effects were performed for the 7.62 cm (3 in.) single sphere only. A plot of the resulting integrated heat flux data obtained is provided as Fig. 10. The

kink in the energy storage histories for the immersion test is an amplified version of the dropping effect of the spherical PCM solid experienced in the dual-latent tests. Due to the increased heat flux and/or length of time required to complete the exchange process, the immersed sphere tests 'dropped' before no later than
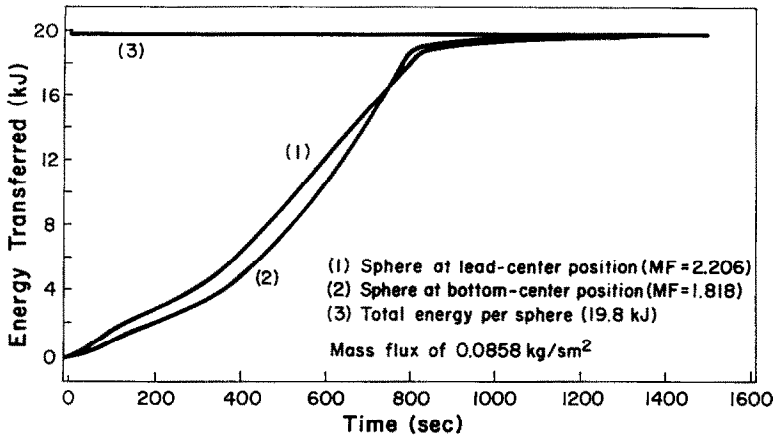
FIG. 11. Integrated heat flux data for $3 \times 3 \times 6$ array of 5.08 cm diameter spheres (data taken at 1 s intervals).

70% of the total time for complete storage. Since this phenomenon had such a significant effect on these tests the useable portions of the data were taken to be the periods of energy storage preceding the release of the PCM solid.

Bed simulation tests. The integrated heat flux data for the $3 \times 3 \times 6$ packed bed experiments is presented in Fig. 11. Two spheres were instrumented at the entry and exit positions of the bed. The figure reveals that for the bed length of six sphere diameters, no significant dependence of the heat transfer rate on the axial position in the bed was detectable. Similar tests to note wall effects were conducted by instrumenting laterally dispersed spheres. Again, no significant temperature variations were noticeable.

It should be noted that though a bed of six sphere diameters is small and may not allow the flow of the working fluid to become fully developed, it is our belief that the heat transfer results given should provide the general information for local behavior in a large bed, particularly those in which the majority of the resistance of transport is associated with the spheres. This is due to the rapid and essentially isothermal condensation of the working fluid.

Visualization study. The test chamber was fitted with polycarbonate flanges at both view port locations so that the condensation process could be visually observed. The predominant mode of condensation viewed was dropwise. A typical visualization photograph is shown in Fig. 12. The visualization study also revealed that the method used to suspend the single spheres during the single sphere tests did not provide the necessary control. It was seen that the sphere would sway in the flow of condensing vapor when the heat exchange process was initiated. This could have caused significant disturbances in the assumed purely natural convection regime of the liquid PCM layer. In addition, condensate from the insulated wire support was seen to run down and off the sphere in question. Though the latter effect was likely small, both were

undesirable and immeasurable, and as a result this portion of the data was not used.

4. NORMALIZED RESULTS, DISCUSSION AND CONCLUSIONS

4.1. *Normalizations*

A normalization technique was employed to reduce the data into a more useful form. The main quantities of interest are the instantaneous energy stored by a given sphere and its particular time of storage. The former could be normalized simply by knowing the total energy storage capacity of the system, or

$$E^* = \frac{E}{E_{\text{scale}}} = \frac{MF \int_{t_i}^{t} q_{\text{exp}} \, dt}{E_{\text{scale}}}. \tag{1}$$

This energy 'scale' is given by

$$E_{\text{scale}} = (mc_p \Delta T)_{\text{shell}} + (mc_{p_s} \Delta T_s + mc_{p_l} \Delta T_l + mh_{\text{sf}})_{\text{pcm}} \tag{2}$$

where $\Delta T_s = T_m - T_i$, $\Delta T_l = T_f - T_m$, and $\Delta T = T_f - T_i$. Subscripts m, s, l, i, and f will imply melt, solid, liquid, initial, and final states, respectively. One can easily see that for charging processes the dimensionless energy storage parameter, E^*, will range between 0 and 1 representing 100% energy storage.

For the normalized time, $t^* = t/t_{\text{scale}}$, t_{scale} may be approximated by a summation of all the individual time scales in the system

$$t_{\text{scale}} \sim t_{\text{conv}} + t_{\text{film}} + t_{\text{shell}} + (t_s + t_l + t_{h_{\text{sf}}})_{\text{pcm}} \tag{3}$$

stemming from the electrically analogous system of resistances in series. Detailed derivation for each term in equation (3) is given in ref. [20]. Next, we assume that (1) the shell wall temperature rapidly exceeds that of the melting point of the PCM as a result of the high heat flux owing to condensation, (2) a heat transfer
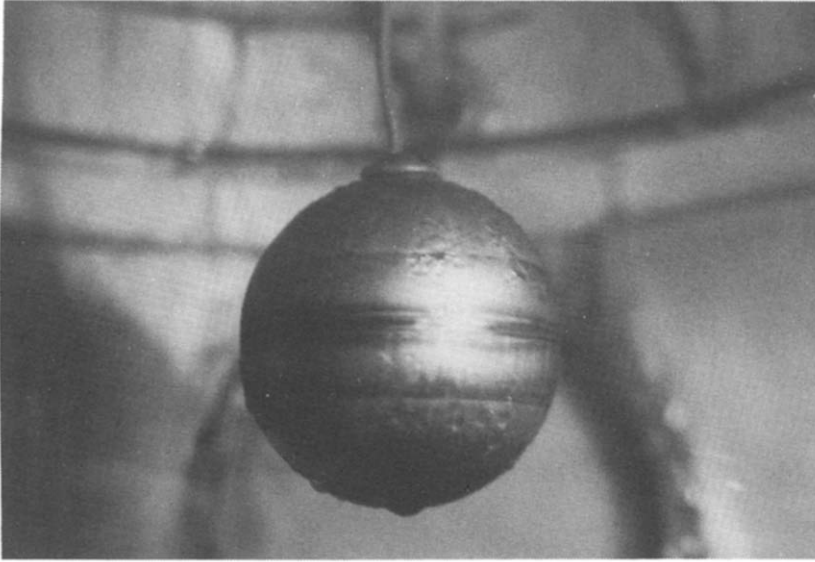
FIG. 12. A typical photograph of steam condensing on a PCM-filled sphere.

coefficient, h, acting between the exterior vapor stream and the sphere surface may be determined, and (3) an effective conductivity, k_{eff}, for the liquid PCM may be calculated to account for the buoyancy-induced convection. In this study, a relationship developed by Scanlan *et al.* [21] was used to estimate the k_{eff}. We further assume the radius of the sphere to be much greater than the thickness of the encapsulating shell $(R \gg X)$. Equation (3) becomes

$$t_{\mathrm{scale}} \sim \frac{E^{\circ}}{R^2}\left(\frac{\ln\dfrac{1}{1-\theta}}{h} + \left(\frac{\delta}{k}\right)_{\mathrm{film}} + \left(\frac{X}{k}\right)_{\mathrm{shell}}\right.$$
$$\left. + \frac{R}{k_{\mathrm{eff}}}\left(\frac{1-\varepsilon_{\mathrm{sph}}^{1/3}}{\varepsilon_{\mathrm{sph}}^{1/3}}\right)\right) \quad (4)$$

where E° is the energy required per degree increase in temperature and is given as

$$E^{\circ} \sim (\rho_1\bar{c}_p)_{\mathrm{pcm}}R^3\left(1 + \frac{3(\rho c_p X)_{\mathrm{shell}}}{(\rho_1\bar{c}_p R)_{\mathrm{pcm}}} + \left(\frac{h_{\mathrm{sf}}}{\bar{c}_p\Delta T}\right)_{\mathrm{pcm}}\right) \quad (5)$$

and ε, the PCM voidage, is given by

$$\varepsilon_{\mathrm{sph}} = 1 - \frac{3m_{\mathrm{pcm}}}{4\pi R^3\rho_{\mathrm{pcm}_s}}. \quad (6)$$

The overbar on the specific heat term appearing in equation (5) implies a phase-corrected value based on temperature, or

$$\bar{c}_p = \frac{c_{p_s}\Delta T_s + c_{p_1}\Delta T_1}{\Delta T}. \quad (7)$$

Noting, typically, for this study and for similar investigations, that $X \ll R$ and that δ_{film} tends to be zero

for the dropwise case, for $\theta = 0.9$ (implying that 95% of the total energy has been stored) and for simplicity $\varepsilon_{\mathrm{sph}} \simeq 0.12$, equation (4) can be reduced to

$$t_{\mathrm{scale}} \sim \frac{E^{\circ}}{R^2}\left(\frac{\ln 10}{h} + \left(\frac{R}{k_{\mathrm{eff}}}\right)_{\mathrm{pcm}_1}\right). \quad (8)$$

For verification purposes, assuming no latent heat transfer $(h_{\mathrm{sf}} = 0)$, equation (8) reduces to $\rho_1 c_p R \times (\ln 10/h + R/k)$ which is the correct scale for the sphere experiencing conduction and convection without phase change. If h and k_{eff} can be determined, the normalized time, $t^* = t/t_{\mathrm{scale}}$, may be calculated for all time. Should the scale relations and accompanying assumptions leading to equation (8) be well posed, the transient storage process for a single sphere under the given conditions should be completed around time $t = t_{\mathrm{scale}}$, or $t^* = 1.0$. Therefore the relationship between E^* and t^* should be one to one at the end of the storage process implying a simple relationship by which all spheres regardless of properties, temperature differences, etc. will generally obey given similar loading conditions. Substituting equation (5) into equation (8) yields the final scale relation

$$t_{\mathrm{scale}} \sim (\rho_1\bar{c}_p)_{\mathrm{pcm}}R\left(1 + \frac{3(\rho c_p X)_{\mathrm{shell}}}{(\rho_1\bar{c}_p R)_{\mathrm{pcm}}} + \left(\frac{h_{\mathrm{sf}}}{\bar{c}_p\Delta T}\right)_{\mathrm{pcm}}\right)$$
$$\times\left(\frac{\ln 10}{h} + \left(\frac{R}{k_{\mathrm{eff}}}\right)\right). \quad (9)$$

It is implied that $k_{\mathrm{eff}} = k_{\mathrm{eff}_{\mathrm{pcm}_1}}$. If it is acceptable that $3(\rho c_p X)_{\mathrm{shell}} \ll (\rho_1\bar{c}_p R)_{\mathrm{pcm}}$ then the normalized time parameter may be reduced to

$$t^* = \frac{t}{t_{\mathrm{scale}}} = \frac{Fo_{\mathrm{eff}}}{(1+Ja^{-1})(2.3Bi_{\mathrm{eff}}^{-1}+1)} \quad (10)$$

where eff denotes an effective quantity employing k_{eff}.
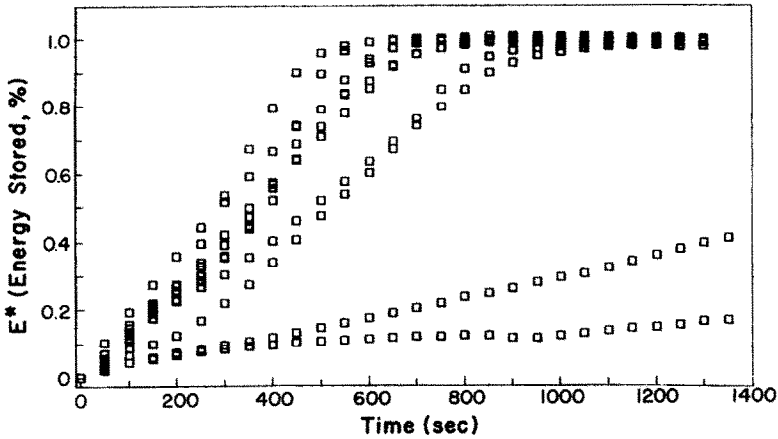
FIG. 13. Plots of normalized energy vs time for total experimental data.

When the sensible storage of the encapsulating shell becomes significant, another term, F, is added to $1 + Ja^{-1}$ in the above equation. This term (F) is represented by

$$F = \frac{(3\rho c_p X)_{\text{shell}}}{(\rho_1 \bar{c}_p R)_{\text{pcm}}}. \tag{11}$$

The normalized energy results of ten experiments representing the breadth of the data collected in this study are plotted in Fig. 13 in real time. These curves represent a wide variety of sphere sizes and steam flow rates. The two lower curves correspond to smaller Stefan numbers. Since an average heat transfer coefficient (h) could be back-calculated from the temperature/time data, k_{eff} remained the only skeptical quantity of the time normalization calculation. A correlation by Scanlan *et al.* [21] was time-averaged in order to determine this quantity. Noting that for $Ste \leqslant 0.1$, $k_{\text{eff}} \simeq k_1$, and that the effective conductivity for the 5.08 cm (2 in.) diameter sphere needed to be reduced 30% for compliance with the 6.35 and 7.62 cm diameter spheres for identical test situations,† the normalizing time calculations were performed on the data of Fig. 13. The result is represented in Fig. 14. The tables of values used in the normalizing calculations are provided as Tables 1 and 2. As is seen, a general collapse is maintained. Review of Fig. 7 indicates that the thickened portion of the collapsed region may simply be due to heat flux measurements made at slightly varying tangential angle locations (referring to Section 2.2). What is clearly indicated by Fig. 14 is the point at which the experiments were completed (i.e. $t^* \simeq 1$), the point of complete thermal

energy storage for the sphere. Regardless of the tangential location of the heat flux measurement this point would result after similar parametric normalization. The slope of this particular collapsed family of energy storage history represents approximately the average surface heat flux for the spheres. Figure 15 shows more specifically the collapse of the data for six tests presented previously.

4.2. Quantification of normalized results

Further simplification of the generalized results can be made by exploiting the linear relationship between E^* and t^*, yielding

$$\frac{E^*}{t^*} = \frac{E}{t} \left(\frac{t_{\text{scale}}}{E_{\text{scale}}} \right) = C_1 \tag{12}$$

where C_1 is some constant $O(1)$. It is understood that E/t is the average energy storage rate (J s^{-1}) for a given sphere and that the process is completed when $E = E_{\text{scale}}$. The average storage rate determined in this manner is very accurate for linear E^* vs t^* relationships. From Fig. 14, C_1 is 0.923—very much $O(1)$. A heat flux relation can then be written

$$q'' = 1.083 \frac{k_{\text{eff}} \Delta T}{R} \left(\frac{1}{2.3 Bi_{\text{eff}}^{-1} + 1} \right) \tag{13}$$

once E^* from equation (1) and t^* from equation (10) are substituted into equation (12) and simplified. This finding appears practically identical in form to the one-dimensional steady state heat flux equation. It should be noted that ε_{sph} was measured and found to be roughly 0.12. Different values will produce a factor multiplying the PCM scale in the denominator of equation (13).

4.3. Potential applications

Very direct applications of the findings presented here may be made. The restrictions of the scaling arguments are primarily associated with the accurate

---

† This may be likely attributable to the range of Scanlan's correlation being nearly exceeded for the 5.08 cm (2 in.) diameter sphere. The two larger sphere sizes collapsed ideally when normalized while the 5.08 cm diameter sphere data scattered. Reduction of k_{eff} calculated by Scanlan's relationship, by 30% brought about the ideal collapse for all of the 5.08 cm sphere data.

FIG. 14. Plots of normalized energy vs normalized time for total experimental data.

Table 2. Experimental values used in calculations of E_{scale} and t_{scale}

Sample file #	Sphere diameter (cm)	$\dot{m}''$ (kg m^{-2} s^{-1})	T_i ($\pm 0.2°$C)	T_f ($\pm 0.2°$C)	E_{tot} (kJ$\pm 4\%$)	h_{ave} (W °C^{-1} m^{-2})	$k_{eff}{}^a$ (W m^{-1} °C^{-1})
51	7.62 (S)	0.293	22.2	106.4	72.7	130.0	0.982
52	7.62 (A)	0.293	23.4	105.0	71.6	106.6	0.976
53	7.62 (A)	0.293	24.2	105.0	71.0	—	—
56	6.35 (S)	0.421	19.5	107.3	42.2	160.0	0.876
57	6.35 (A)	0.421	24.2	104.0	40.0	143.5	0.857
60	5.08 (S)	0.066	21.4	107.0	19.8	173.8	0.749^a
61	5.08 (A)	0.066	21.1	103.0	19.4	155.1	0.741^a
63	5.08 (A)	0.135	18.7	110.3	20.6	190.0	0.760^a
64	5.08 (A)	0.211	18.9	120.7	21.8	230.2	0.785^a
66	5.08 (A)	—	23.2	105.2	—	—	—
67	5.08 (A)	—	18.6	105.5	—	—	—
68	7.62 (I)	Ste = 0.560	23.8	97.9	68.1	87.2	0.954
69	7.62 (I)	Ste = 0.283	23.3	70.4	57.0	206.7	0.772^a
70	7.62 (I)	Ste = 0.103	29.0	54.2	46.5	—	0.667^a

^{a} k_{eff} values determined by Scanlan's correlation which are suspect.
(S), (A), (I) ; single, array, and immersion tests, respectively.
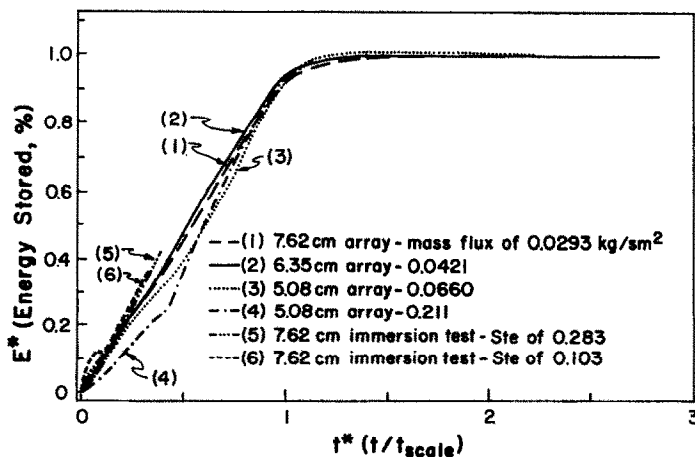
FIG. 15. Plots of normalized energy vs normalized time for various tests.

determination of h and k_{eff}. On Earth, h may be readily obtained, but an accurate value for k_{eff} is difficult to guarantee unless $Ste \leqslant 0.1$. Scanlan's correlation [21] with a time averaging technique was shown to produce reasonable results for the larger sphere sizes tested. In zero gravity environments, the degrees of difficulty are reversed since k_{eff} would simply equal k_1 and h may need to be determined by correlations which apply to zero gravity conditions which are not readily available. Regardless, collapsed solutions are possible with the use of the relationships suggested. The time for a PCM-filled spherical shell to store at least 95% of its thermal energy available may also be determined with reasonable accuracy by

$$t = \frac{0.923 R^2}{\alpha_{\text{eff}}(1 + Ja^{-1})(2.3 Bi_{\text{eff}}^{-1} + 1)} \tag{14}$$

the non-reduced and non-simplified version of which takes the form

$$t = 0.923(\rho \bar{c}_p)_{\text{pcm}} R \left(1 + 3 \frac{(\rho c_p X)_{\text{shell}}}{(\rho c_p R)_{\text{pcm}}} + Ja^{-1} \right)$$

$$\times \left(\frac{\ln 1/(1-\theta)}{h} + \left(\frac{\delta}{k} \right)_{\text{film}} + \left(\frac{X}{k} \right)_{\text{shell}} \right.$$

$$\left. + \frac{R}{k_{\text{eff}}} \left(\frac{1 - \varepsilon^{1.3}}{\varepsilon^{1.3}} \right)_{\text{pcm}} \right). \tag{15}$$

There is no restriction here as to whether or not phase change is occurring in the working fluid. We need to emphasize that the scale relations developed are valid only for the charging process of a single sphere. Thermal design techniques employing these simply stated relations may greatly simplify the method of selection of a PCM bed fitted for a particular thermal operation.

4.4. Conclusions

The scale relationships presented reveal a dimensionless time parameter by which transport rates of spheres regardless of dimensions and thermophysical properties may be correlated. In fact, the relationship discovered was one of the constant heat flux, reasonably accurately determined by the advent of a scaling constant $O(1)$.† Biot numbers in the range of 4–50, Stefan numbers in the range of 0.1–0.6, and Reynolds numbers in the range of 0–50 were tested.

The primary assumptions allowing a time normalization and collapse of the data are that an effective conductivity for the liquid PCM layer (k_{eff}) and a heat transfer coefficient (h) acting between the working fluid and the sphere surfaces can be estimated with reasonable accuracy by existing correlations and/or data.

From the single sphere results (small array tests

were found to be equivalent to single sphere tests) of this study, extension of the above findings can be directly made to incorporate full-scale bed effects, primarily those associated with axial location and energy storage rate dependence thereon.

REFERENCES

1. T. E. W. Schumann, Heat transfer: a liquid flowing through a porous prism, *J. Franklin Inst.* **208**, 405–416 (1928).
2. N. R. Amundson, Solid–fluid interactions in fixed and moving beds: fixed beds with small particles, *Ind. Engng Chem.* **48**, 26–31 (1956).
3. H. Martin, Low Peclet number particle-to-fluid heat and mass transfer in packed beds, *Chem. Engng Sci.* **33**, 913–923 (1978).
4. R. J. Gross, C. E. Hickox and C. E. Hackett, Numerical simulation of dual-media thermal storage system, *J. Solar Energy Engng* **102**, 287–293 (1980).
5. G. F. Robertson and J. C. Cavendish, The effects of flow maldistribution on the thermal response of packed bed converters and thermal energy storage units, ASME Paper 81-HT-59 (1981).
6. A. Shitzer and M. Levy, Transient behavior of a rock bed thermal storage system subject to variable inlet air temperatures: analysis and experimentation, *J. Solar Energy Engng* **105**, 200–211 (1983).
7. A. E. Saez and B. J. McCoy, Transient analysis of packed-bed thermal storage systems, *Int. J. Heat Mass Transfer* **26**, 49–54 (1983).
8. B. A. Peavy and W. E. Dressler, Transpiration heat transfer in thermal energy storage device, National Bureau of Standards Report NBSIR 77-1237, Washington, DC (1977).
9. D. E. Jones and J. E. Hill, Testing of pebble-bed and phase-change thermal energy storage devices according to ASHRAE Standard 94-77, National Bureau of Standards Report NBSIR 79-1737, Washington, DC (1979).
10. D. E. Beasely and J. A. Clark, Transient response of a packed bed for thermal energy storage, *Int. J. Heat Mass Transfer* **27**, 1659–1669 (1984).
11. B. Yimer, J. N. Crisp and E. T. Mahefkey, Transient thermal analysis of phase-change thermal energy storage, ASME Paper 80-HT-2 (1980).
12. M. E. Kordahi, B. Yimer and J. N. Crisp, Transient thermal analysis of phase change thermal energy storage system with density change, ASME Paper 82-HT-10 (1982).
13. H. Torab and D. E. Beasely, Dynamic response of a packed bed of encapsulated PCM, *Proc. 20th Intersociety Energy Conversion Engng Conf.*, Miami Beach, Florida, pp. 313–317 (1985).
14. K. Pal, Heat transfer in a packed bed of spheres filled with a phase change material, Ph.D. thesis, University of Guelph, Canada (1985).
15. A. G. Graves, Transient thermal performance of an experimental packed bed thermal energy storage system, M.S. thesis, University of Tennessee, Knoxville, Tennessee (1985).
16. K. D. Thomas, Direct contact condensation of immiscible fluids in packed beds, M.S. thesis, Department of Mechanical Engineering, University of Utah, Salt Lake City, Utah (1978).

---

† Less dramatically put, the electrically analogous RC time constant was seen to be an effective scaling parameter for this transient thermal situation.

17. P. J. Marto, Recent progress in enhancing film condensation heat transfer on horizontal tubes, *Heat Transfer 1986, Proc. 8th Int. Heat Transfer Conf.*, Vol. 1, pp. 161–170 (1986).

18. J. N. Chung, A numerical simulation of the liquid-metal dual-latent heat packed bed thermal energy storage system, Final Report to AFOSR under 1986 USAF-UES Summer Faculty Research Program (1986).

19. F. E. Moore and Y. Bayazitoglu, Melting within a spherical enclosure, *J. Heat Transfer* **104,** 19–23 (1982).

20. M. M. Weislogel, Heat and mass transfer in a dual-latent thermal energy storage system, M.S. thesis, Washington State University, Pullman, Washington (1988).

21. J. A. Scanlan, E. H. Bishop and R. E. Powe, Natural convection heat transfer between concentric spheres, *Int. J. Heat Mass Transfer* **13,** 1857–1872 (1970).

ETUDE EXPERIMENTALE DE LA CONDENSATION DANS DES PETITS ARRANGEMENTS DE SPHERES EMPLIES DE PCM

Résumé—On conduit des études expérimentales sur le transfert de chaleur et de masse entre un écoulement de vapeur et un petit lit fixe régulier de sphères emplies de PCM (matériau à changement de phase). Les objectifs de la recherche sont d'obtenir les caractéristiques du transfert variable du système de stockage de chaleur latente pendant le processus de charge. Un montage spécial permet l'instrumentation à l'intérieur de la sphère. Il retarde la plongée du PCM solide non fondu, vers le fond de la coquille sphérique, réduisant ainsi la forte dépendance du flux thermique vis-à-vis de la position de l'angle tangentiel. Les transferts thermiques instantanés sont obtenus pour des sphères de trois tailles différentes. On tente d'établir l'influence des nombres de Reynolds et de Stefan sur le transfert des deux phases et sur le stockage d'énergie. Le montage convient bien, particulièrement pour les grandes sphères (6,35 et 7,62 cm de diamètre), ce qui permet d'unifier les énergies normalisées thermiques stockées par une seule échelle de temps adimensionnelle pour tous les essais effectués.

EXPERIMENTELLE UNTERSUCHUNG DER KONDENSATION IN KLEINEN ANORDNUNGEN AUS KUGELN, DIE PHASENWECHSELMATERIAL ENTHALTEN

Zusammenfassung—Es werden experimentelle Untersuchungen des Wärme- und Stofftransports bei der Kondensation von strömendem Dampf in einem kleinen Festbett aus Hohlkugeln, die mit einem Phasenwechselmaterial gefüllt sind, durchgeführt. Das Ziel der Untersuchung ist, das zeitliche Verhalten des Wärme- und Stoffübergangs in einem doppelt-latenten Wärmespeicherungssystem während des Beladungsvorgangs zu ermitteln. Mit Hilfe einer speziellen Vorrichtung wurde das Innere einer Kugel instrumentiert. Diese Vorrichtung verzögert das Absinken des noch ungeschmolzenen Phasenwechselmaterials auf den Boden der Kugelschale, wodurch die starken Unterschiede der Wärmestromdichte am Umfang der Kugel vermindert werden. Für Kugeln mit drei unterschiedlichen Durchmessern wird der zeitlich veränderliche Wärmestrom bestimmt (Einzelkugeln und kleine Festbettanordnungen). Es wurden besondere Versuche ausgeführt, um den Einfluß der Reynolds- und der Stefan-Zahl auf den Zweiphasentransport und die Energiespeicherung zu untersuchen. Die Vorrichtung funktioniert gut, insbesondere mit größeren Kugeln (Durchmesser 6,35 und 7,62 cm). Dies erlaubt die Korrelation der normierten gespeicherten Energie mit Hilfe einer einzigen dimensionslosen Zeitkoordinate.

ЭКСПЕРИМЕНТАЛЬНОЕ ИССЛЕДОВАНИЕ ТЕПЛОПЕРЕНОСА ПРИ КОНДЕНСАЦИИ НА МАЛЫХ УПАКОВКАХ СФЕР, ЗАПОЛНЕННЫХ МАТЕРИАЛОМ С ФАЗОВЫМ ПЕРЕХОДОМ

Аннотация—Экспериментально исследуется тепло- и массоперенос при конденсации водяного пара и небольшим плотным слоем заключенных в капсулы сфер, заполненных материалом с фазовым переходом. Целью исследования является определение переходных характеристик системы аккумуляции скрытой теплоты фазового перехода в процессе загрузки устройства. Внутри сферы используется специальное устройство, которое замедляет опускание нерасплавленного твердого тела, претерпевающего фазовый переход, к основанию сферической оболочки, уменьшая таким образом сильную зависимость теплового потока от тангенциального угла. Получены мгновенные скорости теплопереноса для сфер трех различных размеров. Проводится также экспериментальная проверка зависимостей двухфазного теплообмена и количества аккумулированной энергии от значений чисел Рейнольдса и Стефана. Устройство работало хорошо, особенно в случае больших сфер (диаметром 6,35–7,62 см), что нозволило скоррелировать нормализованную накопленную тепловую энергию для всех проведенных опытов с помощью единичной безразмерной временной шкалы.